materials

MDPI

Article

Comparison of TiO_2 and ZnO for Heterogeneous Photocatalytic Activation of the Peroxydisulfate Ion in Trimethoprim Degradation

Máté Náfrádi [1], Tünde Alapi [1,*], Bence Veres [1], Luca Farkas [1], Gábor Bencsik [2] and Csaba Janáky [2]

[1] Department of Inorganic, Organic and Analytical Chemistry, University of Szeged, Dóm Square 7-8, H-6720 Szeged, Hungary; 7nmate7@gmail.com (M.N.); veres0629@gmail.com (B.V.); fluca@chem.u-szeged.hu (L.F.)

[2] Department of Physical Chemistry and Materials Science, University of Szeged, Aradi Square 1, H-6720 Szeged, Hungary; bencsikg@chem.u-szeged.hu (G.B.); janaky@chem.u-szeged.hu (C.J.)

* Correspondence: alapi@chem.u-szeged.hu

Abstract: The persulfate-based advanced oxidation process is a promising method for degrading organic pollutants. Herein, TiO_2 and ZnO photocatalysts were combined with the peroxydisulfate ion (PDS) to enhance the efficiency. ZnO was significantly more efficient in PDS conversion and $SO_4^{\bullet-}$ generation than TiO_2. For ZnO, the PDS increased the transformation rate of the trimethoprim antibiotic from 1.58×10^{-7} M s^{-1} to 6.83×10^{-7} M s^{-1}. However, in the case of TiO_2, the moderated positive effect was manifested mainly in O_2-free suspensions. The impact of dissolved O_2 and trimethoprim on PDS transformation was also studied. The results reflected that the interaction of O_2, PDS, and TRIM with the surface of the photocatalyst and their competition for photogenerated charges must be considered. The effect of radical scavengers confirmed that in addition to $SO_4^{\bullet-}$, $^{\bullet}OH$ plays an essential role even in O_2-free suspensions, and the contribution of $SO_4^{\bullet-}$ to the transformation is much more significant for ZnO than for TiO_2. The negative impact of biologically treated domestic wastewater as a matrix was manifested, most probably because of the radical scavenging capacity of Cl^- and HCO_3^-. Nevertheless, in the case of ZnO, the positive effect of PDS successfully overcompensates that, due to the efficient $SO_4^{\bullet-}$ generation. Reusability tests were performed in Milli-Q water and biologically treated domestic wastewater, and only a slight decrease in the reactivity of ZnO photocatalysts was observed.

Keywords: advanced oxidation process; peroxydisulfate; matrix effect; domestic wastewater; pharmaceutical

check for updates

Citation: Náfrádi, M.; Alapi, T.; Veres, B.; Farkas, L.; Bencsik, G.; Janáky, C. Comparison of TiO_2 and ZnO for Heterogeneous Photocatalytic Activation of the Peroxydisulfate Ion in Trimethoprim Degradation. *Materials* **2023**, *16*, 5920. https://doi.org/10.3390/ma16175920

Academic Editor: Barbara Pawelec

Received: 26 July 2023
Revised: 23 August 2023
Accepted: 26 August 2023
Published: 29 August 2023

Copyright: © 2023 by the authors. Licensee MDPI, Basel, Switzerland. This article is an open access article distributed under the terms and conditions of the Creative Commons Attribution (CC BY) license (https://creativecommons.org/licenses/by/4.0/).

1. Introduction

Nowadays, environmental pollution, including water pollution, has received particular attention, and treating water pollutants has become an urgent task due to the biologically active and non-biodegradable organic contaminants, such as pharmaceuticals, which cannot be removed entirely using conventional water treatment methods. The global use of antibiotics and the increase of their concentration in wastewater is still growing [1–3]. During wastewater treatment, a significant part of the antibiotics and some of their metabolites can often remain in the effluent and reach surface waters, leading to the emergence of antibiotic-resistant bacterial strains, resulting in more than 70,000 deaths yearly worldwide [4]. Their emergence in wastewater and release to wastewater treatment plants can have significant effects, as they might act as reservoirs of antibiotic-resistant genes [5,6]. Therefore, effective elimination of these contaminants requires additive, tertiary water treatment methods and improvements in the existing technologies.

Advanced oxidation processes (AOPs) based on the in situ generation of strong oxidants have been developed to remove non-biodegradable organic pollutants. Most

AOPs are based on the hydroxyl radical ($^{\bullet}OH$) generation, but in recent years methods based on the sulfate radical ion ($SO_4^{\bullet-}$) have been gaining popularity [7,8]. The $SO_4^{\bullet-}$ has a similar redox potential but a longer lifetime than $^{\bullet}OH$ [9,10]. Moreover, the easy activation of peroxymonosulfate (PMS) and peroxydisulfate (PDS) to produce $SO_4^{\bullet-}$ makes this method favorable. The application of PDS is more advantageous due to its higher oxidation potential, stability, and lower production costs than PMS [11]. From PDS, the $SO_4^{\bullet-}$ can be generated in situ by cleaving the O–O bond, which can be achieved by electron transfer [12,13] or by energy transfer through introducing energy in the form of photons [14,15] or heat [16]. In the case of different AOPs, the application of PDS is often mentioned as an alternative to the application of H_2O_2—the effectiveness of PDS-combined methods can usually exceed the H_2O_2-combined processes, partly due to the higher steady-state concentration of reactive species.

The excitation of the photocatalyst results in charge separation. The photogenerated electrons (e_{CB}^-) and holes (h_{VB}^+) can reduce and oxidize substrates adsorbed on the photocatalyst surface, respectively, or they can recombine with each other and disappear without leading to any chemical reaction. Consequently, an efficient e_{CB}^- scavenger is required to prevent charge recombination and allow oxidation via h_{VB}^+. Most often, dissolved O_2 reacts with e_{CB}^-. The formed $O_2^{\bullet-}$ has a dual role: it can react with organic substances [17,18] or produce $^{\bullet}OH$ via a multistep reaction, especially in the case of TiO_2 and ZnO photocatalysts [19].

In the case of heterogeneous photocatalysis, PDS can act as an e_{CB}^- scavenger, like dissolved O_2. The reaction with the e_{CB}^- results in the formation of $SO_4^{\bullet-}$; its oxidation potential and reactivity significantly exceed that of $O_2^{\bullet-}$. Consequently, the combination of PDS with heterogeneous photocatalysis is expected to enhance the efficiency of the transformation and mineralization of organic substances, as has been confirmed by numerous publications [8,10,12]. PDS has been combined with various photocatalysts, including TiO_2-based composites [20] and metal-oxide-based photocatalysts [21–23]. Its combination with metal-free graphitic carbon nitride (g-C_3N_4) [11] and visible light-active photocatalysts [23] is particularly beneficial.

Nevertheless, the combination of PDS and heterogeneous photocatalysis still raises many questions. The complexity of the process, such as the competition between PDS and O_2, the simultaneous occurrence of radical and non-radical processes, and the interaction of various reactive species with each other, is challenging and needs further investigation [13,20,24–27].

The current research aims to compare the efficiency of commercial TiO_2 and ZnO for removing an antibiotic, trimethoprim (TRIM), and to investigate the efficiency of combined TiO_2/PDS and ZnO/PDS systems. The effects of reaction parameters, the formation of degradation products, the mineralization, and the reaction mechanisms were investigated and compared. Regarding practical applicability, it is essential to examine the matrix effect—for this, biologically purified domestic wastewater was used as a matrix.

2. Materials and Methods

2.1. Materials

The list of used chemicals and solvents can be found in Table S1. Trimethoprim (TRIM) was used as the target substance for photocatalytic test reactions. Air or N_2 gas was applied to control the dissolved O_2 concentration of the treated solution or suspension. To investigate the effect of peroxydisulfate ion ($S_2O_8^{2-}$, PDS), $Na_2S_2O_8$ solution was added to the suspension. Each material was used without further purification. Table S2 shows the data of the biologically treated domestic wastewater (from the water treatment plant, Szeged, Hungary) used as a matrix. Two commercially available photocatalysts, TiO_2 Aeroxide® P25 (Acros Organics; Geel, Antwerp, Belgium) and ZnO (d < 100 nm, Sigma Aldrich; St. Louise, MO, USA) photocatalysts were applied during the experiments. Section 2.4. contains the characterization of the photocatalysts.

2.2. Photoreactors and Experimental Parameters

The photoreactor was equipped with high-power UV-A LED (Vishay; Malvern, USA; VLMU3510-365-130; $LED_{365\ nm}$) emitting 355–380 nm light, with a UV-emission maximum of 365 nm (Figure 1). The 12 SMD diodes were soldered on metal-core printed circuit boards (Meodex; Narbonne, France) and fixed on six aluminum heat sinks (0.70 K W^{-1}; Fischer Elektronik; Lüdenscheid, Germany); two LEDs were fixed on each heat sink. A laboratory power supply (Axiomet; Malmö, Sweden; AX-3005DBL-3, maximum output 5.0 A/30.0 V) provided and controlled the electrical power needed to operate the LEDs (P_{el}^{max} = 21 W). The electrical power was optimized and fixed at 3.4 W. The glass reactor was placed in the center of the apparatus and surrounded by 12 LEDs (Figure 1).

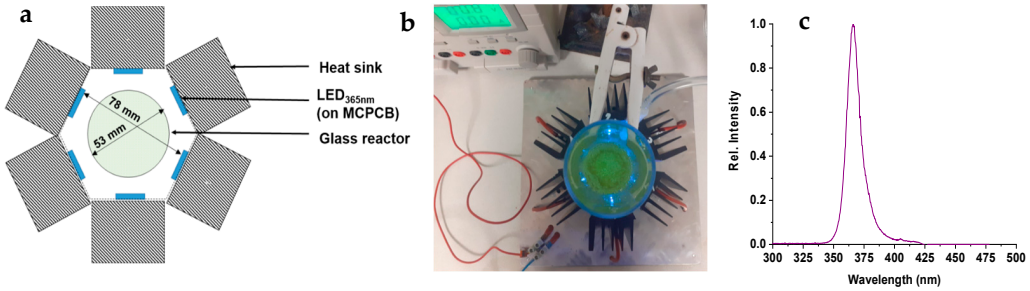


Figure 1. Schematic figure (**a**) and photo (**b**) of the applied photoreactor equipped with LEDs and the emission spectra of the LED (**c**).

In the case of each measurement, a 200 cm^3 suspension was irradiated in a cylindrical borosilicate glass reactor. The dose of the photocatalyst was usually set to 1.0 g dm^{-3}, except when the effect of the photocatalyst dosage was investigated. In that case, it was changed in the 0–1.5 g dm^{-3} range. The concentration of TRIM was 1.0×10^{-4} mol dm^{-3}. The concentration of PDS was varied in the range of 0–5.0 mM, which was set by adding the appropriate volume of 0.5 M PDS stock solution in each case to the 200 mL suspension. The volume of the added stock solution at the highest PDS concentration (5.0×10^{-3} M) was 1.0 mL. The pH of the treated solutions and suspension was not adjusted. To investigate the role of radicals, experiments were performed in the presence of 1.0×10^{-2} M t- BuOH and 1.0×10^{-2} M MeOH.

The suspension was continuously stirred and bubbled with gas (N_2 or synthetic air) during the treatments. The suspension containing photocatalysts and organic target substance was stirred and bubbled in the dark for 30 min to determine the amount of adsorbed target substance. The experiment was started by turning on the light source and adding the PDS solution to the suspension simultaneously. After sampling, 25 µL 0.3 M $Na_2S_2O_3$ solution was added to the sample to decompose the remaining PDS. The photocatalyst samples were centrifuged immediately (Dragonlab; Beijing, China; 15,000 RPM) and filtered with syringe filters (FilterBio; Nantong, China; 0.22 µm, FilterBiO, PVDF-L) before further analysis.

2.3. Characterization of the Light Source

The emission spectra of the LED were measured using a two-channel fiber-optic CCD spectrometer (AvaSpec-FT2048; Avantes, The Netherlands) operated in the 180–880 nm wavelength range. The photon flux of the LEDs was measured using a potassium ferrioxalate actinometer [28]. 1.0×10^{-2} M ferrioxalate solutions were irradiated, and the solutions were bubbled with N_2. The concentration of the released Fe^{2+} was determined after complexation with 1,10-phenanthroline. The concentration of the Fe^{2+}-phenanthroline complex was measured using UV-Vis spectrophotometry (Agilent 8453; Santa Clara, CA, USA). The photon flux of the LED was 1.42×10^{-5} mol_{photon} s^{-1} dm^{-3}, using 3.4 W electric power. The calculated average irradiance (flux density) reaching the reactor wall was approximately 5.6 mW cm^{-2}.

2.4. Characterization of the Photocatalysts

The specific surface area TiO_2 and ZnO was determined and found to be 64 and 13 m^2 g^{-1}, respectively. The average primary particle size for Aeroxide® P25 TiO_2 ranges from 10 to 50 nm, distributed mainly from 15 to 25 nm [29]. For ZnO, this value is 50–70 nm [30]. For TiO_2, the XRD pattern agrees with the results reported in the literature; anatase is the dominant crystal phase in the anatase—rutile mixture [30,31]. The XRD pattern of ZnO confirmed its pure wurtzite phase [32].

Diffuse reflectance spectroscopy (DRS) was performed using an Ocean Optics USB4000 detector and Ocean Optics DH-2000 light source (Figure 2). The band gap energy values of the photocatalysts were evaluated by the Kubelka–Munk approach and the Tauc plot (Figure S1). The calculated band gaps were identical, 3.21 eV for TiO_2 and ZnO (Figure S1).

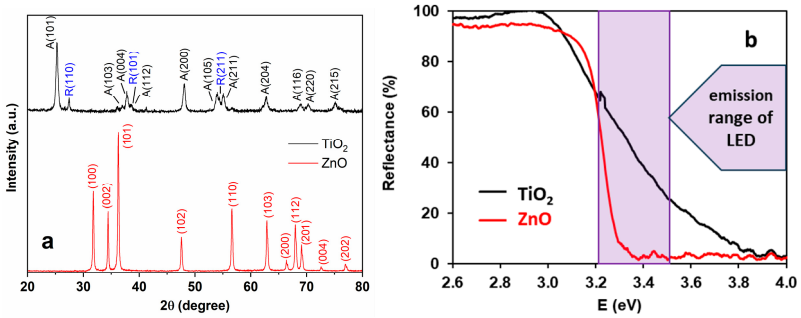


Figure 2. The XRD patterns and Miller indices (A: anatase; R: rutile) (**a**) and the diffuse reflectance spectra of TiO_2 and ZnO (**b**).

2.5. Analytical Methods

The concentration of TRIM was measured by HPLC-DAD (Agilent 1100, Santa Clara, CA, USA; Gemini 3u C6-Phenyl 110A column; Phenomenex; Torrance, CA, USA). The eluent consisted of 10 v/v% methanol and 90 v/v% formate buffer (20 mM, pH = 3.7), the flow rate was 0.4 cm^3 min^{-1}, and the eluent temperature was 40 °C. The detection was performed at 275 nm, and the retention time of TRIM was 7.3 min.

The transformation efficiency of TRIM was characterized by the initial transformation rate (r_0). This value was obtained from the slope of the first-order curve fitted to the points of the initial part of the kinetic curve of TRIM transformation (TRIM concentration (M) versus treatment time (s)). The R^2 value of linear regression was above 0.95. Some experiments were repeated three times to check the reproducibility of the experimental results.

The TRIM degradation products were determined by HPLC-MS, with an Agilent LC/MSD VL mass spectrometer coupled to the HPLC system. The measurements were performed using an ESI ion source and a triple quadruple analyzer in positive mode (3000 V capillary voltage and 80 V fragmentor voltage). The drying gas flow rate was 8.0 dm^3 min^{-1}, and the temperature was 350 °C. The scanned mass range was between 50–1000 AMU. Solid-phase extraction (SPE) was used to remove dissolved inorganic ions before MS measurements. Phenomenex Strata-X, 33 µm cartridges, were used, and after conditioning (0.5 mL methanol and 0.5 mL water) 20 mL sample was loaded. Washing was performed using 1.0 mL water; then, the adsorbed samples were eluted using 0.75 mL methanol.

The sulfate ion (SO_4^{2-}) concentration was measured using ion chromatography (Shimadzu Prominence LC-20AD; Kyoto, Japan; Shodex NI-424 5U column). The eluent contained 2.3×10^{-3} mol dm^{-3} aminomethane, and the flow rate was 1.0 cm^3 min^{-1}.

Total organic carbon (TOC) concentration was determined using an Analytik Jena N/C 3100 analyzer (Analytik Jena; Jena, Germany). The adsorbable organic halogen (AOX) content was measured with a multi-X 2500 analyzer (Analytik Jena). The column method (APU-2) was used for the adsorption of 20 cm^3 samples on 100 mg high-purity activated carbon.

3. Results

3.1. Effect of PDS and Dissolved O_2 on the TRIM Transformation

Using 1.0×10^{-4} M TRIM and 1.0 g dm^{-3} photocatalyst dosage less than 5% of TRIM was adsorbed. The photolysis of TRIM was negligible, and no transformation was observed in the presence of a photocatalyst without irradiation. Using the highest PDS concentration (5.0×10^{-3} M), the slow TRIM transformation took place in the solution without photocatalyst under 365 nm radiation, most probably due to the photolysis of PDS (Figure S2), although its molar absorbance is negligible at this wavelength [7]. The competition with photocatalysts for photons in TiO_2 and ZnO suspensions strongly reduces the possibility of direct PDS photolysis.

The effect of photocatalyst dosage was investigated in the 0–1.5 g dm^{-3} range. The transformation rate of TRIM did not change significantly above 0.5 g dm^{-3} (Figure S2) in the case of both photocatalysts. For further experiments, 1.0 g dm^{-3} TiO_2 and ZnO concentration was used to ensure the complete absorption of the incoming photons by the photocatalyst and to minimize the possibility of direct photolysis of PDS. The TiO_2 was slightly more efficient than ZnO in TRIM transformation (Figure S3), opposite to its less favorable optical properties. The better light absorption property of ZnO can be observed in the wavelength range emitted by $LED_{365\ nm}$ (355–380 nm) (Figure 2b); at 365 nm, TiO_2 reflects approximately 40%, while ZnO practically fully absorbs the photons. The better efficiency of TiO_2 in terms of TRIM transformation can be explained by the more efficient formation of $^{\bullet}OH$, which was verified by Náfrádi [33], comparing TiO_2 and ZnO in the case of coumarin transformation.

The effect of PDS concentration (0–5.0×10^{-3} M) was investigated in aerated suspensions containing 1.0 g dm^{-3} photocatalyst (Figure 3a). For TiO_2, PDS just slightly enhances the transformation rate of TRIM (from 1.72×10^{-7} M s^{-1} to 1.95×10^{-7} M s^{-1}); the effect is moderated, almost negligible. In contrast to TiO_2, in the case of ZnO, the TRIM transformation rate increased significantly from 1.58×10^{-7} M s^{-1} to 6.83×10^{-7} M s^{-1} (Figure 3a). The effect varied according to a saturation curve; above 2.0×10^{-3} M, the efficiency cannot be significantly improved with further increase in PDS concentration. The positive effect is most likely caused by the formation of $SO_4^{\bullet -}$ via electron transfer and its reaction with TRIM. The reactivity of TRIM towards $SO_4^{\bullet -}$ is similar to $^{\bullet}OH$ ($k_{TRIM+^{\bullet}OH} = 8.66 \times 10^9$ M^{-1} s^{-1} [34,35]; $k_{TRIM+SO4^{\bullet -}} = 3.88 \times 10^9$ M^{-1} s^{-1} [35]). The enhancement of mineralization efficiency also could be observed. Due to the addition of 5.0×10^{-3} M PDS to ZnO suspension, the mineralization rate increased and reached the rate measured in the TiO_2 suspension. (Figure 3b). For TiO_2, PDS did not affect the mineralization rate, even at 5.0×10^{-3} M dosage.

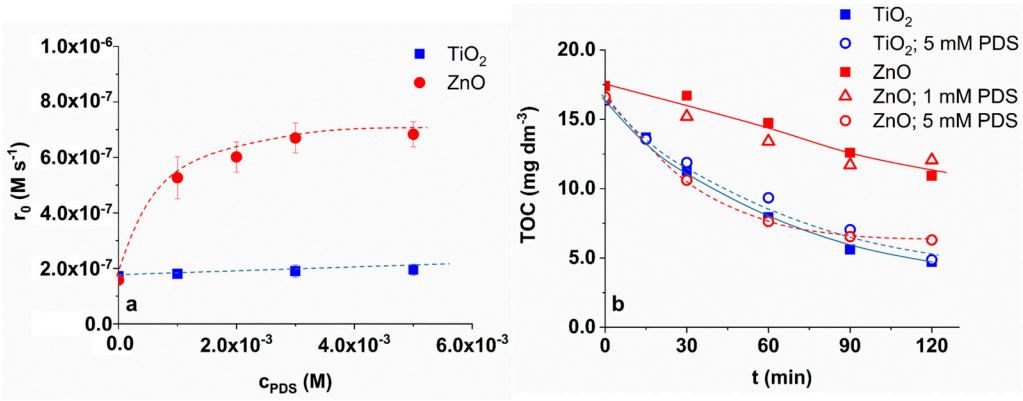


Figure 3. The initial transformation rate (r_0) of TRIM as a function of PDS concentration (**a**) and the change of the total organic carbon (TOC) content using 1.0×10^{-3} M and 5.0×10^{-3} M PDS in aerated suspensions (**b**).

The difference in the surface properties of ZnO and TiO_2 partially explains their different behavior. Under the conditions applied (pH 6.8 and 7.3 for TiO_2 and ZnO suspension, respectively), the surface charge of P25 TiO_2 (pH_{PZC} = 5.2 and pH_{IEP} = 6.2 [36,37] is negative, while the surface charge of ZnO (pH_{PZC} = 8–9.4 [38–41] pH_{IEP} = 6.4–7.5 [42] is positive. For ZnO, a surface interaction was observed for several negative ions (carbonate, sulfate, and phosphate [43–45]), suggesting the possibility of a particular interaction with PDS, which can enhance the electron transfer from the surface of excited ZnO to PDS. However, for TiO_2, no significant interaction was observed between the surface and inorganic anions [38].

Another essential difference between the photocatalysts could be in the $^{\bullet}OH$ formation process and the relative contribution of radical-based reactions and direct charge transfer to the transformation of organic and inorganic substances, which could be especially important for PDS activation. In the case of the anatase phase, $^{\bullet}OH$ formation is related primarily to the e_{CB}^- initiated reduction of O_2 and further transformation of $O_2^{\bullet-}$ [43], while for ZnO, the similar contribution of h_{VB}^+ ($^{\bullet}OH$ formation from H_2O/OH^-) and e_{CB}^- initiated reactions have been suggested [46]. In the case of coumarin transformation, under the same experimental conditions, for ZnO, the direct charge transfer contributed to the transformation to a greater extent than for TiO_2; for the latter, the $^{\bullet}OH$-based transformation was the primary process [33]. Moreover, the higher electronic conductivity of ZnO can result in a more efficient charge accumulation on the surface compared to TiO_2 [33,47,48]. Based on the above mentioned, the reduction of PDS by direct charge transfer on the ZnO surface may be more favorable than on the TiO_2 surface, and its effect on the $^{\bullet}OH$ formation could be different for ZnO and TiO_2.

3.2. Effect of Dissolved O_2 on TRIM Transformation

The fast recombination of photogenerated charges occurs without an effective e_{CB}^- scavenger. The dissolved O_2 usually plays this role. The effect of O_2 was investigated for both catalysts in aerated and O_2-free suspensions, with and without PDS (Figure 4). Without PDS and dissolved O_2, the transformation of TRIM is negligible in both suspensions. However, in the presence of PDS, the transformation occurs even in O_2-free suspensions (Figure 4). PDS greatly enhanced the transformation rate in both O_2-free and aerated ZnO suspensions (Figure 4). While in the case of TiO_2, the effect of PDS depended on the presence of dissolved O_2, it was very slight in the case of aerated but remarkable in the O_2-free suspension (Figure 4). The co-presence of PDS and O_2 and the complexity of their roles can explain the difference between TiO_2 and ZnO.

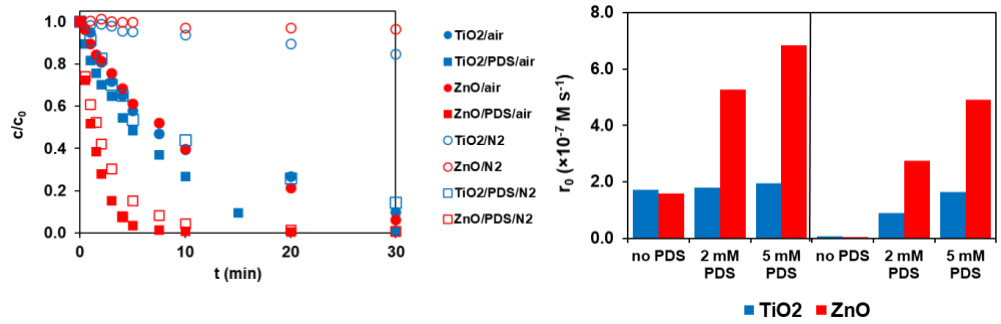


Figure 4. The effect of dissolved O_2 and PDS on the transformation of TRIM in the case of ZnO and TiO_2 in aerated and O_2-free (N_2) suspensions. (**a**: kinetic curves, $c_{PDS} = 5.0 \times 10^{-3}$ M; **b**: initial transformation rates).

The PDS is an excellent e_{CB}^- scavenger that efficiently prevents the recombination of photogenerated charges (e_{CB}^- and h_{VB}^+), enabling the reduction and oxidation of substrates on the surface of photocatalysts. The reaction between PDS and e_{CB}^- results in the facile formation of highly oxidizing $SO_4^{\bullet-}$, which opens a new pathway for the

transformation of TRIM, with a similar rate to $^{\bullet}OH$ [35]. The simultaneous presence of PDS and O_2 can affect the $SO_4^{\bullet-}$ and $O_2^{\bullet-}$ formation rate via competition for e_{CB}^-, and consequently, the transformation rate of organic compounds. The result of the competition also depends on the surface properties of the photocatalysts.

The role of $O_2^{\bullet-}$ is not manifested in a direct reaction with TRIM [34] but in its contribution to $^{\bullet}OH$ formation. For TiO_2 and ZnO, $^{\bullet}OH$ formation partly occurs via the further transformation of $O_2^{\bullet-}$ and H_2O_2 [49]. The $SO_4^{\bullet-}$ also can participate in pH-dependent reactions to produce $^{\bullet}OH$ [50,51], but $^{\bullet}OH$ formation in this way can only become significant above pH 9:

$$SO_4^{\bullet-} + H_2O \rightarrow H^+ + SO_4^{2-} + {}^{\bullet}OH \qquad k = 460\ s^{-1} \tag{1}$$

$$SO_4^{\bullet-} + OH^- \rightarrow SO_4^{2-} + {}^{\bullet}OH \qquad k = 6.5 \times 10^7 \qquad M^{-1}\ s^{-1} \tag{2}$$

Nevertheless, the PDS as an e_{CB}^- scavenger can enhance the $^{\bullet}OH$ formation via h_{VB}^+-driven processes. Thus, in PDS containing TiO_2 and ZnO suspensions, both $SO_4^{\bullet-}$ and $^{\bullet}OH$ can participate in the degradation processes and must be considered a decisive reactive species, even in an O_2-free suspension. Moreover, the increased importance of the direct charge transfer (the reaction between TRIM and photogenerated h_{VB}^+) can be reasonably assumed in the presence of a potent electron scavenger, such as PDS.

The peroxyl radicals (R-$OO^{\bullet}$) produced during the transformation of organic compounds play an important role in their transformations and mineralization—from this point of view, the role of O_2 is unique. For ZnO, the slight positive effect of dissolved O_2 on the transformation of TRIM in the presence of PDS is presumably due to the organic peroxyl radicals, which opens a new path for transformations and simultaneously hinders the backward reactions of carbon-centered radicals. It should also be noted that the reaction between $SO_4^{\bullet-}$ and $^{\bullet}OH$ results in O_2 [52]:

$$SO_4^{\bullet-} + {}^{\bullet}OH \rightarrow H^+ + SO_4^{2-} + 0.5\ O_2 \qquad k = 9.5 \times 10^9 \qquad M^{-1}\ s^{-1} \tag{3}$$

Consequently, O_2-mediated transformation cannot be excluded completely, even in suspension bubbled with N_2.

3.3. Effect of Dissolved O_2 and Trimethoprim on PDS Transformation

Most publications have focused primarily on the transformation of organic compounds and have rarely investigated the PDS transformation. The PDS (2.0×10^{-3} M) transformation was followed by the measurement of SO_4^{2-} concentration. Experiments were conducted in aerated and O_2-free suspensions with and without TRIM (Figure 5).

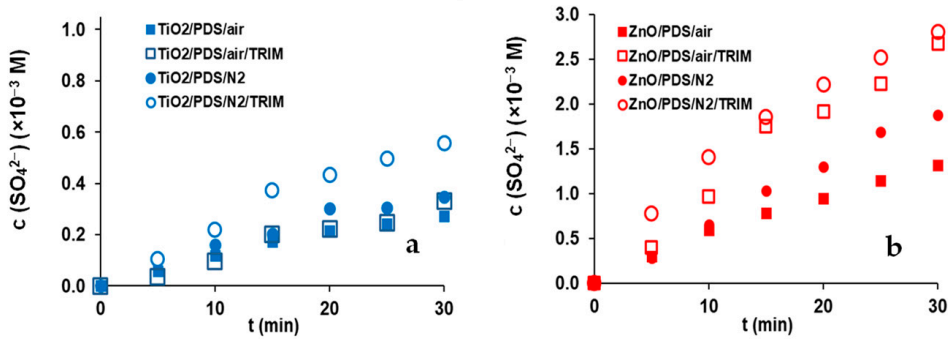


Figure 5. The effect of dissolved O_2 and TRIM (1.0×10^{-4} M) on SO_4^{2-} concentration (c_0(PDS) = 2.0×10^{-3} M) in the case of TiO_2 (**a**) and ZnO (**b**), in aerated and O_2-free (N_2) suspensions.

The SO_4^{2-} formation is significantly faster in ZnO suspension than in TiO_2 suspension (Figure 5, Table S3), especially in the presence of TRIM which is consistent with the effect

of PDS on TRIM transformation (Figure 3) and proves that the PDS transformation is much more favored for ZnO than for TiO_2. Without TRIM, 9% and 12% of PDS were transformed for TiO_2 and 52% and 69% for ZnO in aerated and O_2-free suspension over 60 min treatment, confirming the competition for e_{CB}^- between O_2 and PDS. This competition was much more pronounced in the case of ZnO. In addition to dissolved O_2, TRIM also influenced the transformation of PDS. In an O_2-free TiO_2 suspension, the SO_4^{2-} concentration increased by 70% due to the presence of TRIM; however, this effect was negligible in aerated suspension. In ZnO suspension, the positive impact of TRIM was manifested both in O_2-free and O_2-containing suspensions but still, the extent of the effect depended on the presence of O_2: in an O_2-free suspension 47% increase was achieved, while in an aerated suspension, the SO_4^{2-} concentration was doubled.

In the case of TiO_2-based composite photocatalysts, a positive effect of PDS and PMS on the transformation of organic substances was reported and interpreted by the dual roles of PMS as a surface complexing ligand [53] and a radical precursor. The oxidizing capacity of TiO_2/PMS varied depending on the substrate type [53]. While in the case of dye transformation, photosensitization has an important role [54]. Based on these results, we cannot determine the processes taking place on the surface, but the results do prove that not only the competition between PDS and O_2 but also the interaction of TRIM and PDS with the catalyst surface can affect the transformation. Moreover, depending on the presence of O_2 and photocatalyst properties, different products can form from TRIM, and some of them, such as quinones and phenols, can promote the transformation of PDS [55].

All this suggests that during the combination of PDS and heterogeneous photocatalysis, it may become necessary to consider the interaction of individual materials with the photocatalyst surface or with each other to interpret the processes taking place on the surface and their effect on overall efficiency.

3.4. Effect of Radical Scavengers

The contribution of $^{\bullet}OH$ and $SO_4^{\bullet-}$ to the TRIM transformation was studied by competition kinetics, using radical scavengers. Tert-butanol (t-BuOH) was used as $^{\bullet}OH$ scavenger ($k_{t\text{-}BuOH+\bullet OH} = 6.0 \times 10^8\ M^{-1}\ s^{-1}$ [56]; $k_{t\text{-}BuOH+SO4\bullet-} = 8.0 \times 10^5\ M^{-1}\ s^{-1}$ [57]) and methanol (MeOH) was applied as $^{\bullet}OH$ ($k_{MeOH+\bullet OH} = 9.7 \times 10^8\ M^{-1}\ s^{-1}$ [56,57] and $SO_4^{\bullet-}$ ($k_{MeOH+SO4\bullet-} = 2.0 \times 10^7\ M^{-1}\ s^{-1}$ [57,58]) scavenger. Comparing their effect, the contribution of $^{\bullet}OH$ and $SO_4^{\bullet-}$ to the transformation of TRIM ($k_{TRIM+\bullet OH} = 8.66 \times 10^9\ M^{-1}\ s^{-1}$ [34,35]; $k_{TRIM+SO4\bullet-} = 3.88 \times 10^5\ M^{-1}\ s^{-1}$ [35]) can be estimated. Experiments were performed in the presence of 1.0×10^{-2} M t-BuOH and MeOH. Both alcohols theoretically scavenge ~90% of $^{\bullet}OH$ (RSC $\approx$ 0.91 and MeOH reacts with ~20% of $SO_4^{\bullet-}$.

Without PDS, the inhibition effect of t-BuOH and MeOH confirms the significant contribution of $^{\bullet}OH$-based transformation (Figure 6), especially for ZnO. Samy et al. [59] supposed the h_{VB}^+-driven TRIM transformation in TiO_2 suspension, which can explain the lower inhibitory effect of radical scavengers (Figure 6). Using 2.0×10^{-3} M PD, in aerated suspension, there is no difference between the effect of t-BuOH and MeOH for TiO_2, underlining that the $^{\bullet}OH$ remains the dominant reaction partner. The moderated inhibition effect of t-BuOH can be observed in O_2-free suspension and at higher (5 mM) PDS concentration.

For ZnO, the effect of MeOH exceeds that of t-BuOH, proving the significant contribution of $SO_4^{\bullet-}$ to the TRIM transformation (Figure 6). The inhibition effect of t-BuOH and MeOH is less pronounced in the presence of PDS (opposite to TiO_2, when PDS did not change the r_0/r_0^{REF} value, especially in the case of MeOH), suggesting that the overall contribution of radical-based transformation probably became suppressed while other processes could also participate in the TRIM transformation. In several cases, the formation and significant contribution of $^1O_2$ to the transformation was confirmed in PDS-containing systems [13,23,60]. $^1O_2$ reacts with TRIM ($3.2 \times 10^6\ M^{-1}\ s^{-1}$ [31]), however, more slowly than $^{\bullet}OH$ and $SO_4^{\bullet-}$.

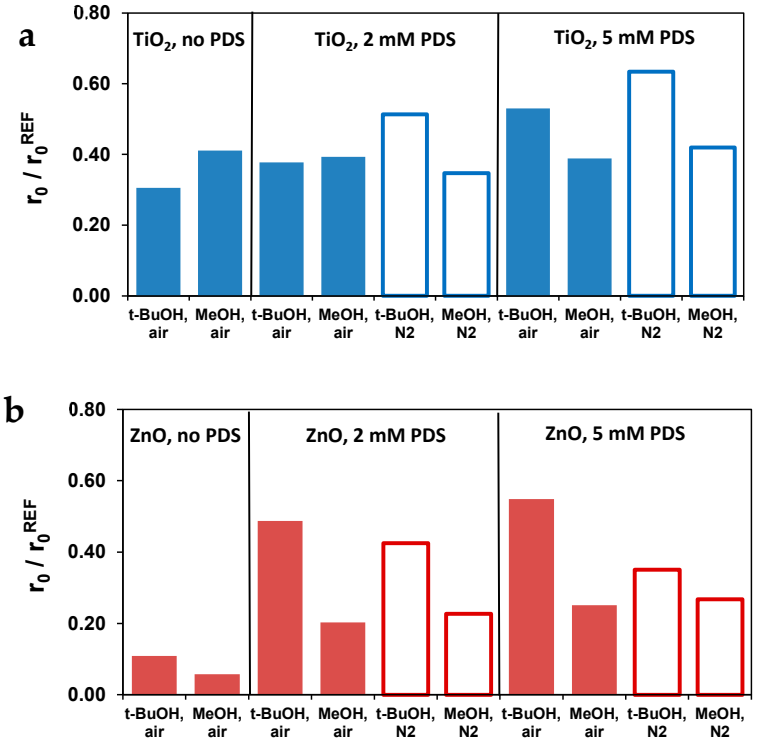


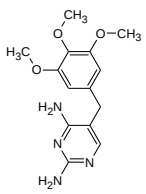
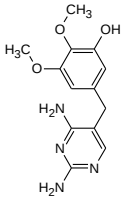
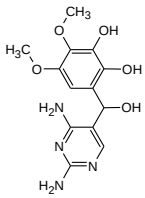
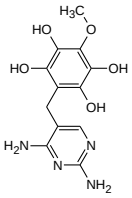
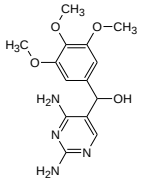
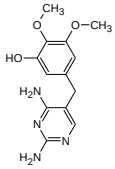
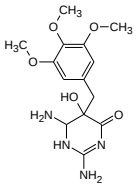
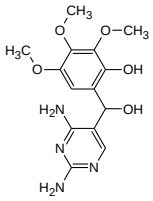
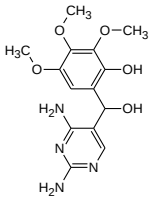
Figure 6. The relative initial transformation rates of TRIM in the presence of t-BuOH and MeOH at different PDS concentrations in the case of TiO_2 (**a**) and ZnO (**b**). (r_0^{REF}: the initial transformation rate without radical scavenger; r_0: the initial transformation rate in the presence of radical scavenger).

The effect of radical scavengers is consistent with our previous results; the transformation of PDS and, consequently, the contribution of $SO_4^{\bullet-}$ based reaction is more favored for ZnO than TiO_2. The effect of t-BuOH confirms that $^{\bullet}OH$ plays an essential role in the presence of PDS, even in O_2-free suspensions. Moreover, the results of the competition tests also pointed out that, in addition to radical processes, the role of $^1O_2$ can be considerable in the case of the ZnO/PDS method.

3.5. Aromatic Intermediates of TRIM Transformation

Organic compounds react with $SO_4^{\bullet-}$ and $^{\bullet}OH$; the differences lie in the preferred reaction pathway and the reaction kinetics [61,62]. The formed products were identified based on HPLC-MS (Table 1) and compared with previously published results [59,63–65]. For TRIM, the $^{\bullet}OH$ reacts primarily by addition to the aromatic ring (TRIM-OH) or via H-abstraction with -CH_2- bridge, while $SO_4^{\bullet-}$ prefers to react by electron-transfer reactions and results in keto-trimethoprim (TRIM=O) besides hydroxylated products. In the case of TiO_2 and ZnO, the same aromatic products were formed with and without PDS, but their concentration distribution was different (Figures S4 and S6). The main reaction pathways were demethylation (P1, P2, and P4) and hydroxylation of the 1,2,3-trimethoxybenzene (P1, P2a, P2b, P4). Without PDS for TiO_2, primarily P2, P3, and P4 form due to the hydroxylation and demethylation, while for ZnO, P6 was the main product; in addition to that, P4 and P8 form but P2 and P7, the dihydroxylation products were not detected (Figures S4 and S6). The difference reflects the distinct contribution of $^{\bullet}OH$-based reaction and direct charge transfer. The PDS did not significantly change the product distribution (Figures S4–S7); therefore, reactions with $SO_4^{\bullet-}$ most likely result in similar products like $^{\bullet}OH$.

Table 1. The m/z value and structure of aromatic products of TRIM.

Name	TRIM	P1	P2a	P2b	P3
Structure					
t_{ret} (min)	9.5	2.5	3.1	3.1	3.5
m/z (AMU)	291.2	277.2	309.2	295.2	307.2
Name	P4	P5	P6	P7	P8
Structure					
t_{ret} (min)	3.7	5.1	5.6	6.9	7.3
m/z (AMU)	277.2	only DAD detection	325.3	323.2	307.2

3.6. Matrix Effect

Experiments were performed in biologically treated domestic wastewater (BTWW) as a mild matrix (Figure 7) having a relatively low TOC value but high Cl^- and HCO_3^- content (Table S2). Both organic substances and inorganic ions can act as radical scavengers, affecting the TRIM transformation rate via competition for reactive species. The changes in the surface properties of the photocatalyst due to the presence of inorganic ions can affect the efficiency of charge separation and radical formation [66–71]. In addition, the contribution of secondary radicals formed from inorganic ions ($^{\bullet}Cl$ and $CO_3^{\bullet-}$) must also be considered. The matrix effect was investigated without and in the presence of PDS.

In the case of TiO_2, the TRIM transformation and mineralization rate was significantly reduced in BTWW both with and without PDS (Figure 7 and Table 2). Using ZnO, the matrix practically does not affect the transformation and slightly decreases the mineralization rate without PDS (Figure 7b). The different inhibitory effect of BTWW suggests that the reason is most likely not the organic content of the matrix and its reaction with $^{\bullet}OH$ but the presence of inorganic components and their different interactions with the surface of TiO_2 and ZnO. All this impacts the processes taking place on the surface of the photocatalysts and consequently determines the formation of radicals, the overall efficiency of the catalyst, and the transformation of organic substances.

For ZnO, in the presence of PDS, the transformation and mineralization of TRIM is most probably initiated primarily by $SO_4^{\bullet-}$. As a result of the matrix, the transformation and mineralization rate decreased in this case as well, but its extent was much smaller than in the case of TiO_2 (Figure 7 and Table 2). Comparing the initial transformation rates measured in Milli-Q and matrix, in the case of TiO_2, it was reduced to 1.6×10^{-8} M s^{-1} without PDS, while to 4.0×10^{-8} M s^{-1} in the presence of PDS. Similarly, these values for ZnO are 1.7×10^{-7} M s^{-1} without PDS and 3.33×10^{-7} M s^{-1} in the presence of PDS. The latter is more than two times higher than the TRIM transformation rate in Milli-Q without PDS (1.58×10^{-7} M s^{-1}) (Table 2). Although the matrix effect cannot be eliminated, the positive impact of PDS in the case of ZnO compensates for it and can even overcompensate. It is noteworthy, however, that in the presence of PDS, the negative impact of inorganic ions and the matrix is more pronounced. Without PDS, HCO_3^- reduces the transformation rate

by only 10%, while in the presence of PDS, it decreases it by nearly 40%. Similarly, BTWW results in a reduction only in the presence of PDS. A plausible explanation for this is the change in the radical set; due to the longer half-life of $SO_4^{\bullet -}$ (30–40 µs in comparison to 20 ns of $^{\bullet}OH$ [9,10]), the TRIM transformation is more likely to occur in the aqueous phase than on the ZnO surface. This can have consequences, such as an increased manifestation of the radical scavenging effect of inorganic ions.

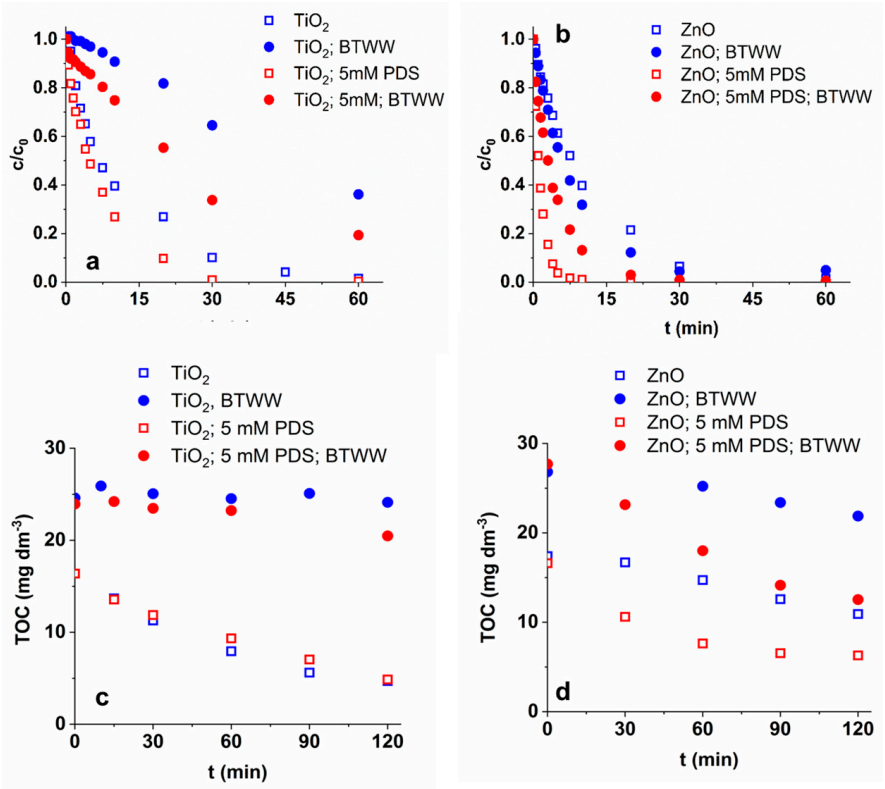


Figure 7. The effect of BTWW on the transformation (**a**,**b**) and mineralization (**c**,**d**) efficiency without and with PDS, in the case of TiO_2 (**a**,**c**) and ZnO (**b**,**d**).

Table 2. The initial transformation rate of TRIM in MQ-water, in the presence of Cl^- (120 mg dm^{-3}) HCO_3^- (525 mg dm^{-3}), and in BTWW (c_{PDS} = 5.0 × 10^{-3} M).

	r_0 (×10^{-7} M s^{-1})			
	TiO_2	**TiO_2/PDS**	**ZnO**	**ZnO/PDS**
MQ	1.72	1.95	1.58	6.83
Cl^-	1.43	1.40	1.56	5.18
HCO_3^-	1.03	1.27	1.39	4.08
Cl^- + HCO_3^-	1.05	1.25	1.45	4.72
BTWW	0.16	0.40	1.70	3.33
	r_0^{BTWW}/r_0^{MQ}			
	0.06	0.21	1.08	0.49

The effect of the two most abundant anions, Cl^- (120 mg dm^{-3}) and HCO_3^- (525 mg dm^{-3}), was investigated using the same concentrations as in BTWW (Table 2). TiO_2 was more sensitive than ZnO to the presence of ions, especially to HCO_3^- without PDS. In the presence of PDS, the inhibitory effect of inorganic ions was similar for the two catalysts (Table 2), with reference to the change in transformation processes and probably the increase in the contribution of radical-based processes.

HCO_3^- may act as $^\bullet OH$ and $SO_4^{\bullet-}$ scavenger and also react with h_{VB}^+. The reaction with $^\bullet OH$ and $SO_4^{\bullet-}$ results in the formation of less reactive, selective carbonate radicals ($CO_3^{\bullet-}$) [66]:

$$HCO_3^- + {}^\bullet OH \rightarrow CO_3^{\bullet-} + H_2O \qquad k = 1.0 \times 10^7\ M^{-1}\ s^{-1} \tag{4}$$

$$HCO_3^- + SO_4^{\bullet-} \rightarrow CO_3^{\bullet-} + SO_4^{2-} + H^+ \qquad k = 2.8 \times 10^6\ M^{-1}\ s^{-1} \tag{5}$$

The reaction between HCO_3^- and h_{VB}^+ also results in $CO_3^{\bullet-}$ formation [66,67]:

$$HCO_3^- + h_{VB}^+ \rightarrow CO_3^{\bullet-} + H^+ \tag{6}$$

Using coumarin as the target substance, the impact of HCO_3^- on the mineralization rate was observed in TiO_2 suspension; this effect was moderated for ZnO [33]. Results were explained by the reaction between HCO_3^- and h_{VB}^+, which is more significant in the case of TiO_2 than in the case of ZnO. For ZnO, the HCO_3^- primarily acts as a $^\bullet OH$ scavenger in the aqueous phase. TRIM reacts with $CO_3^{\bullet-}$ with a lower reaction rate ($1.3 \times 10^7\ M^{-1}\ s^{-1}$ [72]) than $^\bullet OH$ and $SO_4^{\bullet-}$, thus HCO_3^- results in inhibition, especially for TiO_2.

Cl^- has a much stronger radical scavenging capacity than HCO_3^-, as is reflected in their reaction rate constants (7)–(11). At the pH of the measurements (pH < 7), the further transformation of $Cl^\bullet$ and various reactive chlorine species (RCS) result in the reformation of $^\bullet OH$ (10) [73,74], which could be the reason that the negative impact of Cl^- manifests itself less than expected:

$$Cl^- + {}^\bullet OH \rightarrow Cl^\bullet + OH^- \qquad k = 4.3 \times 10^9\ M^{-1}\ s^{-1} \tag{7}$$

$$Cl^\bullet + Cl^- \rightarrow Cl_2^{\bullet-} \qquad k = 7.8 \times 10^9\ M^{-1}\ s^{-1} \tag{8}$$

$$Cl^\bullet / Cl_2^{\bullet-} + H_2O \rightarrow ClOH^{\bullet-} + H^+ \ / + Cl^- \tag{9}$$

$$ClOH^{\bullet-} \rightarrow {}^\bullet OH + Cl^- \tag{10}$$

$$Cl^- + SO_4^{\bullet-} \rightarrow Cl^\bullet + SO_4^{2-} \qquad k = 3.6 \times 10^8\ M^{-1}\ s^{-1} \tag{11}$$

In PDS containing suspensions, the negative effect of Cl^- is similar to HCO_3^-, most probably due to the intensive decrease of $SO_4^{\bullet-}$ concentration.

In the presence of both anions, the reaction between RCS and HCO_3^- must be taken into consideration [73,75]:

$$Cl^\bullet + HCO_3^- \rightarrow CO_3^{\bullet-} + Cl^- \qquad k = 2.8 \times 10^8\ M^{-1}\ s^{-1} \tag{12}$$

$$Cl_2^{\bullet-} + HCO_3^- \rightarrow CO_3^{\bullet-} + 2\ Cl^- + H+ \qquad k = 8.0 \times 10^7\ M^{-1}\ s^{-1} \tag{13}$$

The products may reflect the changes in the radical set (Figures S4–S7). In the case of TiO_2, both HCO_3^- and Cl^- changed the product distribution, especially in the presence of PDS (Figures S4 and S5). The selectivity of $CO_3^{\bullet-}$ probably caused the enhanced formation of hydroxylated products [76,77]. This effect is less pronounced for ZnO (Figures S6 and S7). Despite its negligible impact on the TRIM transformation rate, Cl^- changed the formation of degradation products. In the case of TiO_2, the amount of the P4 demethylated product increased, while the hydroxylated P3 was not detected. A similar increase in P4 was observed in the presence of PDS. For ZnO, Cl^- impacts product distribution; the formation of P3 significantly increased, which might imply a change in the reaction mechanism, most likely due to the RCS.

3.7. Reusability

From a practical point of view, it is essential to investigate the change in the activity of the catalyst and its structural stability. Due to the increased efficiency, the reusability of the ZnO photocatalysts was investigated over three runs. The catalyst was not washed between successive cycles; at the beginning of each cycle, 2.0×10^{-3} M PDS and 1.0×10^{-4} M TRIM were added to the suspension. Experiments were performed in MQ-water and BTWW matrix (Figure 8).

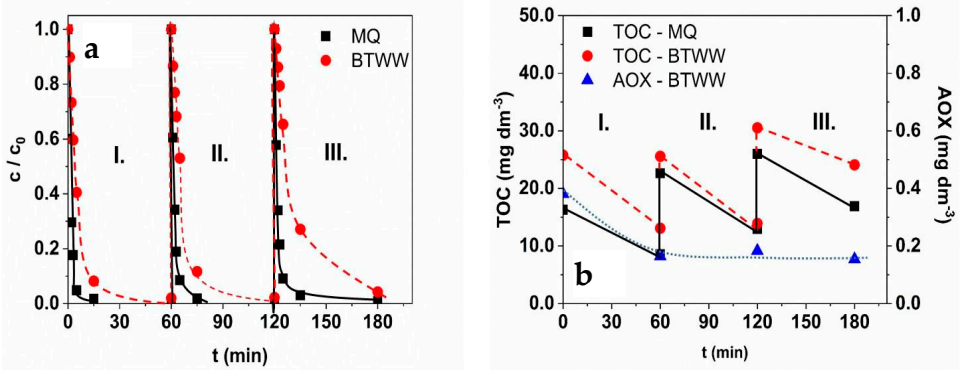


Figure 8. The relative concentration of TRIM (**a**) and the TOC and AOX content (**b**) over three consecutive cycles in MQ water and BTWW matrix.

In Milli-Q water, the transformation rate of TRIM decreased slightly (6.02×10^{-7} M s^{-1} $\rightarrow$ 5.18×10^{-7} M s^{-1} $\rightarrow$ 5.37×10^{-7} M s^{-1}), most probably due to the products accumulated in the treated suspension, as is demonstrated by the TOC values determined at the end of each cycle (Figure 8).

In BTWW, the transformation was slower and reduced in each run by 15–20% (2.03×10^{-7} M s^{-1} $\rightarrow$ 1.72×10 M^{-1} s^{-1} $\rightarrow$ 1.10×10^{-7} M s^{-1}), most likely due to the similar reason as in Milli-Q water (Figure 8). Due to the Cl^- content of the matrix and the possibility of RCS generation, the adsorbable organic halogen (AOX) content was measured, as reactions with RCS, especially with $Cl^{\bullet}$ and $Cl_2^{\bullet -}$ can lead to the formation of halogenated organics. The initial AOX content of BTWW (0.4 mg dm^{-3}) was reduced during the first cycle and did not exceed 0.17 mg dm^{-3} (Figure 8b). The result confirms that in the case of the PDS-combined ZnO-based heterogeneous photocatalytic process, the halogenation of organic substances is not significant even in a matrix with a high Cl^- content and low organic content. The decrease in catalyst activity is presumably attributable to the combined effect of the matrix and the accumulated products, which can be mitigated with appropriate treatment time and regeneration of the catalyst surface. The results of XRD and DRS measurements proved no characteristic change in the catalyst's structure during treatments, even in the presence of PDS and inorganic ions.

4. Conclusions

In this work, the commercially available photocatalysts, TiO_2 and ZnO, were combined with the peroxydisulfate ion (PDS) to enhance the charge separation and generate sulfate radical ion ($SO_4^{\bullet -}$). Trimethoprim antibiotic was used as the target substance to investigate the PDS-assisted heterogeneous photocatalysis. Significant differences were found between the efficiency of ZnO and TiO_2 for PDS activation and, consequently, for trimethoprim transformation. For ZnO, in both aerated and O_2-free suspensions, the PDS significantly increased the transformation rate; however, in the case of TiO_2, the positive effect was manifested in O_2-free suspensions. The impact of dissolved O_2 and trimethoprim on PDS transformation suggested that the interaction of individual materials with the photocatalyst surface and each other is necessary to interpret the processes on the surface and their effect on the overall efficiency. The impact of radical scavengers confirmed that $^{\bullet}$OH plays an

essential role in the presence of PDS even in O_2-free suspensions, while the contribution of $SO_4^{\bullet -}$ to the transformation is much more significant for ZnO than for TiO_2.

The biologically treated domestic wastewater was used to investigate the matrix effect. TiO_2 was very sensitive to the impact of the matrix and its HCO_3^- content; both the transformation and mineralization rate of TRIM were inhibited, while for ZnO, this effect was moderated. Most probably, the inhibition is attributed to the radical scavenging capacity of inorganic components, such as Cl^- and HCO_3^-, and their effect on the surface properties of the photocatalysts. The PDS cannot eliminate the impact of the matrix, but its positive effect on the transformation rate of TRIM can compensate for and even exceed that in the case of ZnO.

Supplementary Materials: The following supporting information can be downloaded at: https://www.mdpi.com/article/10.3390/ma16175920/s1, Table S1: The list of the chemicals, their manufacturer/distributors, and purity. Table S2: The measured parameters of the biologically treated domestic wastewater (BTWW). Figure S1: Tauc-plot analysis for determination of the band-gap value of TiO_2 and ZnO photocatalysts. Figure S2: The relative concentration of TRIM during 365 nm photolysis, in the presence of 5.0×10^{-3} M PDS in the dark and under 365 nm irradiation (without catalyst), and the effect of 1.0×10^{-2} M SO_4^{2-}. Figure S3: The initial reaction rate (r_0) of TRIM as a function of suspension concentration. Table S3: The initial formation rate (r_0) of SO_4^{2-}, and the R^2 values of the linear fitting used for the determination r_0 values (c0(TRIM) = 1.0×10^{-4} M and c_0(PDS) = 2.0×10^{-3} M). Figure S4: Formation of degradation products during heterogeneous photocatalysis with TiO_2 photocatalyst. Figure S5: Formation of degradation products during PDS-assisted heterogeneous photocatalysis with TiO_2 photocatalyst. Figure S6: Formation of degradation products during heterogeneous photocatalysis with ZnO photocatalyst. Figure S7: Formation of degradation products during PDS-assisted heterogeneous photocatalysis with ZnO photocatalyst.

Author Contributions: Investigations, writing—original draft preparation: M.N. Conceptualization, writing—original draft preparation, review and editing, funding acquisition: T.A. Investigation: B.V., M.N. and L.F. Ion-chromatography measurements: C.J. and G.B. All authors have read and agreed to the published version of the manuscript.

Funding: This work was financed by the National Research, Development, and Innovation Office—NKFI Fund OTKA, project number FK132742. Tünde Alapi, thanks for the support of the János Bolyai Research Scholarship of the Hungarian Academy of Sciences. Luca Farkas (ÚNKP-22-3-SZTE-398) and Bence Veres (ÚNKP-23-1-SZTE) thanks to the New National Excellence Program of the Ministry for Culture and Innovation from the source of the National Research, Development, and Innovation Fund.

Institutional Review Board Statement: Not applicable.

Informed Consent Statement: Not applicable.

Data Availability Statement: The data is included in the article or Supplementary Materials.

Acknowledgments: The authors thank the Szegedi Vízmű Zrt. for providing the biologically treated domestic wastewater as a matrix.

Conflicts of Interest: The authors declare no conflict of interest.

References

1. Uddin, T.M.; Chakraborty, A.J.; Khusro, A.; Zidan, B.R.M.; Mitra, S.; Emran, T.B.; Dhama, K.; Ripon, M.K.H.; Gajdács, M.; Sahibzada, M.U.K.; et al. Antibiotic Resistance in Microbes: History, Mechanisms, Therapeutic Strategies and Future Prospects. *J. Infect. Public. Health* **2021**, *14*, 1750–1766. [CrossRef] [PubMed]
2. Romandini, A.; Pani, A.; Schenardi, P.A.; Pattarino, G.A.C.; De Giacomo, C.; Scaglione, F. Antibiotic Resistance in Pediatric Infections: Global Emerging Threats, Predicting the near Future. *Antibiotics* **2021**, *10*, 393. [CrossRef] [PubMed]
3. Tiwari, A.; Kurittu, P.; Al-Mustapha, A.I.; Heljanko, V.; Johansson, V.; Thakali, O.; Mishra, S.K.; Lehto, K.M.; Lipponen, A.; Oikarinen, S.; et al. Wastewater Surveillance of Antibiotic-Resistant Bacterial Pathogens: A Systematic Review. *Front. Microbiol.* **2022**, *13*, 977106. [CrossRef] [PubMed]
4. Hou, J.; Long, X.; Wang, X.; Li, L.; Mao, D.; Luo, Y.; Ren, H. Global Trend of Antimicrobial Resistance in Common Bacterial Pathogens in Response to Antibiotic Consumption. *J. Hazard. Mater.* **2023**, *442*, 130042. [CrossRef]

5. Manaia, C.M.; Rocha, J.; Scaccia, N.; Marano, R.; Radu, E.; Biancullo, F.; Cerqueira, F.; Fortunato, G.; Iakovides, I.C.; Zammit, I.; et al. Antibiotic Resistance in Wastewater Treatment Plants: Tackling the Black Box. *Environ. Int.* **2018**, *115*, 312–324. [CrossRef] [PubMed]
6. Kumar, A.; Pal, D. Antibiotic Resistance and Wastewater: Correlation, Impact and Critical Human Health Challenges. *J. Environ. Chem. Eng.* **2018**, *6*, 52–58. [CrossRef]
7. Stefan, M.I. Sulfate Radical Ion—Based AOPs. In *Advanced Oxidation Processes for Water Treatment: Fundamentals and Applications*; IWA Publishing: London, UK, 2017; pp. 429–460.
8. Lee, J.; Von Gunten, U.; Kim, J.H. Persulfate-Based Advanced Oxidation: Critical Assessment of Opportunities and Roadblocks. *Environ. Sci. Technol.* **2020**, *54*, 3064–3081. [CrossRef]
9. Li, H.; Shang, J.; Yang, Z.; Shen, W.; Ai, Z.; Zhang, L. Oxygen Vacancy Associated Surface Fenton Chemistry: Surface Structure Dependent Hydroxyl Radicals Generation and Substrate Dependent Reactivity. *Environ. Sci. Technol.* **2017**, *51*, 5685–5694. [CrossRef]
10. Oh, W.D.; Dong, Z.; Lim, T.T. Generation of Sulfate Radical through Heterogeneous Catalysis for Organic Contaminants Removal: Current Development, Challenges and Prospects. *Appl. Catal. B* **2016**, *194*, 169–201. [CrossRef]
11. Hasija, V.; Nguyen, V.H.; Kumar, A.; Raizada, P.; Krishnan, V.; Khan, A.A.P.; Singh, P.; Lichtfouse, E.; Wang, C.; Thi Huong, P. Advanced Activation of Persulfate by Polymeric G-C_3N_4 Based Photocatalysts for Environmental Remediation: A Review. *J. Hazard. Mater.* **2021**, *413*, 125324. [CrossRef]
12. Brienza, M.; Katsoyiannis, I.A. Sulfate Radical Technologies as Tertiary Treatment for the Removal of Emerging Contaminants from Wastewater. *Sustainability* **2017**, *9*, 1604. [CrossRef]
13. He, S.; Chen, Y.; Li, X.; Zeng, L.; Zhu, M. Heterogeneous Photocatalytic Activation of Persulfate for the Removal of Organic Contaminants in Water: A Critical Review. *ACS ES T Eng.* **2022**, *2*, 527–546. [CrossRef]
14. Gao, Y.Q.; Gao, N.Y.; Deng, Y.; Yang, Y.Q.; Ma, Y. Ultraviolet (UV) Light-Activated Persulfate Oxidation of Sulfamethazine in Water. *Chem. Eng. J.* **2012**, *195–196*, 248–253. [CrossRef]
15. Saien, J.; Osali, M.; Soleymani, A.R. UV/Persulfate and UV/Hydrogen Peroxide Processes for the Treatment of Salicylic Acid: Effect of Operating Parameters, Kinetic, and Energy Consumption. *Desalination Water Treat.* **2015**, *56*, 3087–3095. [CrossRef]
16. Ji, Y.; Xie, W.; Fan, Y.; Shi, Y.; Kong, D.; Lu, J. Degradation of Trimethoprim by Thermo-Activated Persulfate Oxidation: Reaction Kinetics and Transformation Mechanisms. *Chem. Eng. J.* **2016**, *286*, 16–24. [CrossRef]
17. Ngo Thi, T.D.; Nguyen, L.H.; Nguyen, X.H.; Phung, H.V.; The Vinh, T.H.; Van Viet, P.; Van Thai, N.; Le, H.N.; Pham, D.T.; Van, H.T.; et al. Enhanced Heterogeneous Photocatalytic Perozone Degradation of Amoxicillin by ZnO Modified TiO_2 Nanocomposites under Visible Light Irradiation. *Mater. Sci. Semicond. Process* **2022**, *142*, 106456. [CrossRef]
18. Ma, J.; Zhou, H.; Yan, S.; Song, W. Kinetics Studies and Mechanistic Considerations on the Reactions of Superoxide Radical Ions with Dissolved Organic Matter. *Water Res.* **2019**, *149*, 56–64. [CrossRef]
19. Nosaka, Y.; Nosaka, A.Y. Generation and Detection of Reactive Oxygen Species in Photocatalysis. *Chem. Rev.* **2017**, *117*, 11302–11336. [CrossRef]
20. Ge, M.; Hu, Z.; Wei, J.; He, Q.; He, Z. Recent Advances in Persulfate-Assisted TiO_2-Based Photocatalysis for Wastewater Treatment: Performances, Mechanism and Perspectives. *J. Alloys Compd.* **2021**, *888*, 161625. [CrossRef]
21. Alapi, T.; Veres, B.; Náfrádi, M.; Farkas, L.; Pap, Z.; Covic, A. Application of BiOX Photocatalyst to Activate Peroxydisulfate Ion-Investigation of a Combined Process for the Removal of Organic Pollutants from Water. *Catalysts* **2023**, *13*, 513. [CrossRef]
22. Oh, W.D.; Lim, T.T. Design and Application of Heterogeneous Catalysts as Peroxydisulfate Activator for Organics Removal: An Overview. *Chem. Eng. J.* **2019**, *358*, 110–133. [CrossRef]
23. Tian, D.; Zhou, H.; Zhang, H.; Zhou, P.; You, J.; Yao, G.; Pan, Z.; Liu, Y.; Lai, B. Heterogeneous Photocatalyst-Driven Persulfate Activation Process under Visible Light Irradiation: From Basic Catalyst Design Principles to Novel Enhancement Strategies. *Chem. Eng. J.* **2022**, *428*, 131166. [CrossRef]
24. Chen, G.; Yu, Y.; Liang, L.; Duan, X.; Li, R.; Lu, X.; Yan, B.; Li, N.; Wang, S. Remediation of Antibiotic Wastewater by Coupled Photocatalytic and Persulfate Oxidation System: A Critical Review. *J. Hazard. Mater.* **2021**, *408*, 124461. [CrossRef] [PubMed]
25. Sabri, M.; Habibi-Yangjeh, A.; Khataee, A. Nanoarchitecturing TiO_2/$NiCr_2O_4$ p-n Heterojunction Photocatalysts for Visible-Light-Induced Activation of Persulfate to Remove Tetracycline Hydrochloride. *Chemosphere* **2022**, *300*, 134594. [CrossRef] [PubMed]
26. Yang, J.; Zhu, M.; Dionysiou, D.D. What Is the Role of Light in Persulfate-Based Advanced Oxidation for Water Treatment? *Water Res.* **2021**, *189*, 116627. [CrossRef] [PubMed]
27. Lin, D.; Fu, Y.; Li, X.; Wang, L.; Hou, M.; Hu, D.; Li, Q.; Zhang, Z.; Xu, C.; Qiu, S.; et al. Application of Persulfate-Based Oxidation Processes to Address Diverse Sustainability Challenges: A Critical Review. *J. Hazard. Mater.* **2022**, *440*, 129722. [CrossRef]
28. Hatchard, C.G.; Parker, C.A. A New Sensitive Chemical Actinometer II. Potassium Ferrioxalate as a Standard Chemical Actinometer. *Proc. R. Soc. Lond. Ser. A* **1956**, *A235*, 518–536. [CrossRef]
29. Zuccheri, T.; Colonna, M.; Stefanini, I.; Santini, C.; Di Gioia, D. Bactericidal Activity of Aqueous Acrylic Paint Dispersion for Wooden Substrates Based on TiO_2 Nanoparticles Activated by Fluorescent Light. *Materials* **2013**, *6*, 3270–3283. [CrossRef]
30. White, L.; Koo, Y.; Yun, Y.; Sankar, J. TiO_2 Deposition on AZ31 Magnesium Alloy Using Plasma Electrolytic Oxidation. *J. Nanomater.* **2013**, *2013*, 319437. [CrossRef]

31. Thamaphat, K.; Limsuwan, P.; Ngotawornchai, B. Phase Characterization of TiO_2 Powder by XRD and TEM. *Agric. Nat. Resour.* **2008**, *42*, 357–361.
32. Arefi, M.R.; Rezaei-Zarchi, S. Synthesis of Zinc Oxide Nanoparticles and Their Effect on the Compressive Strength and Setting Time of Self-Compacted Concrete Paste as Cementitious Composites. *Int. J. Mol. Sci.* **2012**, *13*, 4340–4350. [CrossRef]
33. Náfrádi, M.; Alapi, T.; Bencsik, G.; Janáky, C. Impact of Reaction Parameters and Water Matrices on the Removal of Organic Pollutants by TiO_2/LED and ZnO/LED Heterogeneous Photocatalysis Using 365 and 398 nm Radiation. *Nanomaterials* **2022**, *12*, 5. [CrossRef] [PubMed]
34. Luo, X.; Zheng, Z.; Greaves, J.; Cooper, W.J.; Song, W. Trimethoprim: Kinetic and Mechanistic Considerations in Photochemical Environmental Fate and AOP Treatment. *Water Res.* **2012**, *46*, 1327–1336. [CrossRef]
35. Luo, Y.; Su, R.; Yao, H.; Zhang, A.; Xiang, S.; Huang, L. Degradation of Trimethoprim by Sulfate Radical-Based Advanced Oxidation Processes: Kinetics, Mechanisms, and Effects of Natural Water Matrices. *Environ. Sci. Pollut. Res.* **2021**, *28*, 62572–62582. [CrossRef]
36. Zeng, M. Influence of TiO_2 Surface Properties on Water Pollution Treatment and Photocatalytic Activity. *Bull. Korean Chem. Soc.* **2013**, *34*, 953–956. [CrossRef]
37. Kosmulski, M. The Significance of the Difference in the Point of Zero Charge between Rutile and Anatase. *Adv. Colloid. Interface Sci.* **2002**, *99*, 255–264. [CrossRef]
38. Degen, A.; Kosec, M. Effect of pH and Impurities on the Surface Charge of Zinc Oxide in Aqueous Solution. *J. Eur. Ceram. Soc.* **2000**, *20*, 667–673. [CrossRef]
39. Le, A.T.; Syuhada, N.; Samsuddin, B.; Chiam, S.-L.; Pung, S.-Y. Synergistic Effect of pH Solution and Photocorrosion of ZnO Particles on the Photocatalytic Degradation of Rhodamine B. *Bull. Mater. Sci.* **2021**, *44*, 5. [CrossRef]
40. Taylor, Z.; Marucho, M. The Self-Adaptation Ability of Zinc Oxide Nanoparticles Enables Reliable Cancer Treatments. *Nanomaterials* **2020**, *10*, 269. [CrossRef]
41. Fatehah, M.O.; Aziz, H.A.; Stroll, S. Stability of ZnO Nanoparticles in Solution. Influence of pH, Dissolution, Aggregation and Disaggregation Effects. *J. Colloid. Sci. Biotechnol.* **2014**, *3*, 75–84. [CrossRef]
42. Rao, S.R.; Finch, J.A. Base Metal Oxide Flotation Using Long Chain Xanthates. *Int. J. Miner. Process.* **2003**, *69*, 251–258. [CrossRef]
43. Do, T.H.; Nguyen, V.T.; Nguyen, Q.D.; Chu, M.N.; Ngo, T.C.Q.; Van Tan, L. Equilibrium, Kinetic and Thermodynamic Studies for Sorption of Phosphate from Aqueous Solutions Using Zno Nanoparticles. *Processes* **2020**, *8*, 1397. [CrossRef]
44. Liu, C.-F.; Lu, Y.-J.; Hu, C.-C. Effects of Anions and PH on the Stability of ZnO Nanorods for Photoelectrochemical Water Splitting. *ACS Omega* **2018**, *3*, 3429–3439. [CrossRef]
45. Janusz, W. Specific Adsorption of Carbonate Ions at the Zinc Oxide/Electrolyte Solution Interface Article in Physicochemical Problems of Mineral Processing. *Physicochem. Probl. Miner. Process.* **2008**, *42*, 57–66.
46. Chen, Q.; Wang, H.; Luan, Q.; Duan, R.; Cao, X.; Fang, Y.; Ma, D.; Guan, R.; Hu, X. Synergetic Effects of Defects and Acid Sites of 2D-ZnO Photocatalysts on the Photocatalytic Performance. *J. Hazard. Mater.* **2020**, *385*, 121527. [CrossRef] [PubMed]
47. Baxter, J.B.; Schmuttenmaer, C.A. Conductivity of ZnO Nanowires, Nanoparticles, and Thin Films Using Time-Resolved Terahertz Spectroscopy. *J. Phys. Chem. B* **2006**, *110*, 25229–25239. [CrossRef]
48. Meulenkamp, E.A. Electron Transport in Nanoparticulate ZnO Films. *J. Phys. Chem. B* **1999**, *103*, 7831–7838. [CrossRef]
49. Hwang, J.Y.; Moon, G.h.; Kim, B.; Tachikawa, T.; Majima, T.; Hong, S.; Cho, K.; Kim, W.; Choi, W. Crystal Phase-Dependent Generation of Mobile OH Radicals on TiO_2: Revisiting the Photocatalytic Oxidation Mechanism of Anatase and Rutile. *Appl. Catal. B* **2021**, *286*, 119905. [CrossRef]
50. Neta, P.; Madhavan, V.; Zemel, H.; Fessenden, R.W. Rate Constants and Mechanism of Reaction of Sulfate Radical Anion with Aromatic Compounds. *J. Am. Chem. Soc.* **1977**, *99*, 163–164. [CrossRef]
51. Yu, X.-Y.; Bao, Z.-C.; Barker, J. Free Radical Reactions Involving $Cl^{\bullet}$, $Cl_2^{-\bullet}$, and $SO_4^{-\bullet}$ in the 248 nm Photolysis of Aqueous Solutions Containing $S_2O_8^{2-}$ and Cl^-. *J. Phys. Chem. A* **2003**, *35*, 295–308. [CrossRef]
52. Klaning, U.K.; Sehested, K.; Appelman, E.H. Laser Flash Photolysis and Pulse Radiolysis of Aqueous Solutions of the Fluoroxysulfate Ion, SO_4F^-. *Inorg. Chem.* **1991**, *30*, 3582–3584. [CrossRef]
53. Jo, Y.; Kim, C.; Moon, G.H.; Lee, J.; An, T.; Choi, W. Activation of Peroxymonosulfate on Visible Light Irradiated TiO_2 via a Charge Transfer Complex Path. *Chem. Eng. J.* **2018**, *346*, 249–257. [CrossRef]
54. Chen, X.; Wang, W.; Xiao, H.; Hong, C.; Zhu, F.; Yao, Y.; Xue, Z. Accelerated TiO_2 Photocatalytic Degradation of Acid Orange 7 under Visible Light Mediated by Peroxymonosulfate. *Chem. Eng. J.* **2012**, *193–194*, 290–295. [CrossRef]
55. Fang, G.; Gao, J.; Dionysiou, D.D.; Liu, C.; Zhou, D. Activation of Persulfate by Quinones: Free Radical Reactions and Implication for the Degradation of PCBs. *Environ. Sci. Technol.* **2013**, *47*, 4605–4611. [CrossRef] [PubMed]
56. Buxton, G.V.; Greenstock, C.L.; Helman, W.P.; Ross, A.B. Critical Review of Rate Constants for Reactions of Hydrated Electrons, Hydrogen Atoms and Hydroxyl Radicals ($^{\bullet}OH/^{\bullet}O^-$ in Aqueous Solution. *J. Phys. Chem. Ref. Data* **1988**, *17*, 513–886. [CrossRef]
57. Hu, L.; Wang, P.; Shen, T.; Wang, Q.; Wang, X.; Xu, P.; Zheng, Q.; Zhang, G. The Application of Microwaves in Sulfate Radical-Based Advanced Oxidation Processes for Environmental Remediation: A Review. *Sci. Total Environ.* **2020**, *722*, 137831. [CrossRef]
58. Heckel, E. Pulsradiolytische Untersuchung Des Radikal-Anions SO_4^{2-}. *Angew. Chem.* **1966**, *78*, 779. [CrossRef]
59. Samy, M.; Ibrahim, M.G.; Gar Alalm, M.; Fujii, M.; Ookawara, S.; Ohno, T. Photocatalytic Degradation of Trimethoprim Using S-TiO_2 and Ru/WO_3/ZrO_2 Immobilized on Reusable Fixed Plates. *J. Water Process Eng.* **2020**, *33*, 101023. [CrossRef]

60. Liu, J.; Ding, C.; Gong, S.; Fu, K.; Deng, H.; Shi, J. Enhanced Degradation of Antibiotic by Peroxydisulfate Catalysis with CuO@CNT: Simultaneous $^1O_2$ Oxidation and Electron-Transfer Regime. *Molecules* **2022**, *27*, 7064. [CrossRef]
61. Scaria, J.; Nidheesh, P.V. Comparison of Hydroxyl-Radical-Based Advanced Oxidation Processes with Sulfate Radical-Based Advanced Oxidation Processes. *Curr. Opin. Chem. Eng.* **2022**, *36*, 100830. [CrossRef]
62. Xia, X.; Zhu, F.; Li, J.; Yang, H.; Wei, L.; Li, Q.; Jiang, J.; Zhang, G.; Zhao, Q. A Review Study on Sulfate-Radical-Based Advanced Oxidation Processes for Domestic/Industrial Wastewater Treatment: Degradation, Efficiency, and Mechanism. *Front. Chem.* **2020**, *8*, 592056. [CrossRef] [PubMed]
63. Sirtori, C.; Agüera, A.; Gernjak, W.; Malato, S. Effect of Water-Matrix Composition on Trimethoprim Solar Photodegradation Kinetics and Pathways. *Water Res.* **2010**, *44*, 2735–2744. [CrossRef] [PubMed]
64. Cai, Q.; Hu, J. Decomposition of Sulfamethoxazole and Trimethoprim by Continuous UVA/LED/TiO_2 Photocatalysis: Decomposition Pathways, Residual Antibacterial Activity and Toxicity. *J. Hazard. Mater.* **2017**, *323*, 527–536. [CrossRef] [PubMed]
65. Zhang, Z.; Yang, Q.; Wang, J. Degradation of Trimethoprim by Gamma Irradiation in the Presence of Persulfate. *Radiat. Phys. Chem.* **2016**, *127*, 85–91. [CrossRef]
66. Farner Budarz, J.; Turolla, A.; Piasecki, A.F.; Bottero, J.Y.; Antonelli, M.; Wiesner, M.R. Influence of Aqueous Inorganic Anions on the Reactivity of Nanoparticles in TiO_2 Photocatalysis. *Langmuir* **2017**, *33*, 2770–2779. [CrossRef]
67. Kaabeche, O.N.E.H.; Zouaghi, R.; Boukhedoua, S.; Bendjabeur, S.; Sehili, T. A Comparative Study on Photocatalytic Degradation of Pyridinium-Based Ionic Liquid by TiO_2 and ZnO in Aqueous Solution. *Int. J. Chem. React. Eng.* **2019**, *17*, 20180253. [CrossRef]
68. Lair, A.; Ferronato, C.; Chovelon, J.M.; Herrmann, J.M. Naphthalene Degradation in Water by Heterogeneous Photocatalysis: An Investigation of the Influence of Inorganic Anions. *J. Photochem. Photobiol. A Chem.* **2008**, *193*, 193–203. [CrossRef]
69. Šojić Merkulov, D.V.; Lazarević, M.J.; Despotović, V.N.; Banić, N.D.; Finčur, N.L.; Maletić, S.P.; Abramović, B.F. The Effects of Inorganic Anions and Organic Matter on Mesotrione (Callisto®) Removal from Environmental Waters. *J. Serbian Chem. Soc.* **2017**, *82*, 343–355. [CrossRef]
70. Bouanimba, N.; Laid, N.; Zouaghi, R.; Sehili, T. A Comparative Study of the Activity of TiO_2 Degussa P25 and Millennium PCs in the Photocatalytic Degradation of Bromothymol Blue. *Int. J. Chem. React. Eng.* **2018**, *16*, 20170014. [CrossRef]
71. Cheng, Z.; Kok Eng, T.; Tao, Y.; Eng Ting, K.; Jiang Yin, X. Studies of Photocatalytic Kinetics on the Degradation of Bisphenol a (BPA) by Immobilized ZnO Nanoparticles in Aerated Photoreactors. *J. Environ. Sci. Eng. A* **2012**, *1*, 187–194.
72. Wojnárovits, L.; Tóth, T.; Takács, E. Rate Constants of Carbonate Radical Anion Reactions with Molecules of Environmental Interest in Aqueous Solution: A Review. *Sci. Total Environ.* **2020**, *717*, 137219. [CrossRef]
73. Stefan, M.I. UV/Chlorine Process. In *Advanced Oxidation Processes for Water Treatment: Fundamentals and Applications*; IWA Publishing: London, UK, 2017; pp. 383–428.
74. Khan, S.; He, X.; Khan, J.A.; Khan, H.M.; Boccelli, D.L.; Dionysiou, D.D. Kinetics and Mechanism of Sulfate Radical- and Hydroxyl Radical-Induced Degradation of Highly Chlorinated Pesticide Lindane in UV/Peroxymonosulfate System. *Chem. Eng. J.* **2017**, *318*, 135–142. [CrossRef]
75. Mertens, R.; yon Sonntag, C. Photolysis (λ = 254 nm) of Tetrachloroethene in Aqueous Solutions. *J. Photochem. Photobiol. A Chem.* **1995**, *85*, 1–9. [CrossRef]
76. Dell'Arciprete, M.L.; Soler, J.M.; Santos-Juanes, L.; Arques, A.; Mártire, D.O.; Furlong, J.P.; Gonzalez, M.C. Reactivity of Neonicotinoid Insecticides with Carbonate Radicals. *Water Res.* **2012**, *46*, 3479–3489. [CrossRef] [PubMed]
77. Mazellier, P.; Busset, C.; Delmont, A.; De Laat, J. A Comparison of Fenuron Degradation by Hydroxyl and Carbonate Radicals in Aqueous Solution. *Water Res.* **2007**, *41*, 4585–4594. [CrossRef]

Disclaimer/Publisher's Note: The statements, opinions and data contained in all publications are solely those of the individual author(s) and contributor(s) and not of MDPI and/or the editor(s). MDPI and/or the editor(s) disclaim responsibility for any injury to people or property resulting from any ideas, methods, instructions or products referred to in the content.